IEEE Access
Multidisciplinary | Rapid Review | Open Access Journal

Received November 18, 2016, accepted December 21, 2016, date of publication January 11, 2017, date of current version August 22, 2017.

Digital Object Identifier 10.1109/ACCESS.2017.2651742

Interactive Multiple Model Filter for Land-Mobile Satellite Communications at Ka-Band

PAULO VICTOR RODRIGUES FERREIRA[1], RANDY PAFFENROTH[2], AND ALEXANDER M. WYGLINSKI[1], (Senior Member, IEEE)

[1]Department of Electrical and Computer Engineering, Worcester Polytechnic Institute, Worcester, MA 01605, USA
[2]Department of Mathematical Sciences and Data Science, Worcester Polytechnic Institute, Worcester, MA 01605 USA

Corresponding author: Alexander M. Wyglinski (alexw@wpi.edu)

This work was supported by the Brazilian Federal Agency CAPES through the Science without Borders Scholarship Program under Grant BEX 18701/12-4.

ABSTRACT In this paper, an Interactive Multiple Model filter design is proposed to improve signal shadowing detection performance on land-mobile channels during rain fading for a downlink operating at Ka-band through a geostationary satellite. A robust solution for on-line determination of the filter measurement error covariance is provided. Analyses are performed for a combination of channels under different atmospheric conditions, clear sky and rain, and different scenarios, suburban and rural. Using International telecommunications union-based synthesized attenuation time-series, the proposed filter achieved a reduction in the incorrect detection duration of 32% for the scenario with a mobile terminal experiencing rain, and by 60% for the scenario with a fixed terminal experiencing rain.

INDEX TERMS Interacting multiple model, Ka-band, Kalman filter, land mobile radio, satellite communication, shadowing, rain fading.

I. INTRODUCTION

High speed Internet access via satellite networks is increasingly attracting more attention, especially for communities that do not possess reliable access to terrestrial broadband communication options [1]. In order to keep up customer demand, a growing number of satellite Internet operators are planning to use or have already started using higher frequency bands, such as the Ka-band (26–40 GHz) [2]. These higher frequency satellite communication bands possess more spectrum availability, thus allowing for transmission links with wider bandwidths to be offered as well as accommodating more links at higher connection speeds [3]. Consequently, high-throughput satellite communication system designs are employing innovative solutions such as additional payload flexibility via software-defined radio (SDR) in order to enable dynamic resource allocation, *i.e.*, flexible power and spectrum allocation [4], and adaptive coding and modulation (ACM) [5]–[7], also used for channel impairment mitigation. Impairments affecting the signal line-of-sight (LOS), *e.g.* fading and shadowing, are functions of the space and atmospheric weather, operational frequency band, terminal location and motion speed for the case of land-mobile satellite (LMS) systems, and environment type, *e.g.*, rural, urban, suburban, and hilly terrain. Correct detection of an impairment event in the presence of multiple impairment events might lead to a more effective response of mitigation techniques [8] and/or actions that minimizes its impact on the QoS [9]–[11].

One component commonly used by schemes that attempt to minimize or mitigate these signal impairments is the knowledge of the communications channel state information (CSI). A common CSI element is signal-to-noise ratio (SNR) [12], [13] measured at the receiver that can be used locally by open-loop implementations, or fed back to the transmitter when a closed-loop solution is implementation. Communication signals passing through geostationary satellites (GEO) experience large propagation delays due to the high orbits associated with GEO satellites, which are around 36, 000 km, resulting in round-trip times (RTT) of more than 0.5 second between two ground stations (GS). Compared to this RTT, different channel attenuation sources present different dynamics, *e.g.*, atmospheric fading, mostly caused by rain, is a slow process with time correlation of more than 10 seconds [8], [12], thus, CSI prediction would not be useful for mitigation of slow events given the relatively long channel coherence time. On the other hand, multipath fading characteristic of LMS channels, such as those caused by signal reflections, and atmospheric scintillation, considered

fast fading events, possess a time correlation on the order of milliseconds or less [12]. Given that this time correlation is shorter than the GEO RTT, the CSI cannot be estimated and fed back fast enough since it would be outdated at the moment of this usage. However, signal shadowing, another well studied event present on LMS channels [14]–[16], is neither a very fast nor very slow process, and could be tracked for reconfiguration control purposes [17]. Its dynamics vary according to the terminal location, motion speed, as well as with the relative satellite location in the sky [15]. One unique characteristic of signal shadowing is that it is basically deep fading experienced by both transmitter and receiver, at the same time, causing communication outage for that specific link. Based on this fact, an open-loop detection scheme is expected to properly track the occurrence of signal shadowing. Additionally, [14], reported that for LMS channels at Ka-band, shadowing is the most severe impairment due to its signal shorter wavelength causing it to be more scattered than reflected, resulting in LOS blockage.

Future cognitive satellite links through LMS channels may benefit from shadowing detectors to enable more power savings, spectrum sharing improvements, and better network relay selection mechanisms when mobile terminals experience clear sky or rainy conditions. These detectors should be robust enough to operate under different weather conditions. Since shadowing causes link outage, fading mitigation techniques are not effective. Thus, the nodes should refrain from transmitting during shadowing events, allowing power to be saved at all link nodes: mobile terminal(s), gateway, and satellite. As a consequence, transmissions between these nodes should stop at the same time. If collaborative nodes are located within the range of those primary nodes that shut down, spectrum sharing could potentially be exploited during that silence time duration. In addition to saving power and making spectrum available, network relay selection mechanisms [11], [18] may achieve a better throughput and latency performance by rerouting packets at time instants that are more accurately determined. Also, for systems not capable of relaying packets, either by its network architecture or unavailability of relaying nodes, data could be buffered during shadowing events and transmitted later on, avoiding an increase in network load and latency caused by unnecessary retransmissions, representing another way of saving power and sharing spectrum.

In the literature, there are several shadowing detectors that have been proposed. In [19] a fish-eye camera was employed for good/bad channel state detection and compared it with an SNR threshold detector as in [20]–[22]. In [23] the mean SNR was used for shadowing detection to assist ACM in LMS channels at 2 GHz, while in [24] the same detection method was used but did not specify the carrier frequency band. In [11] and [25] the mean SNR was used to control relay selection mechanisms in terrestrial wireless networks. In [9] shadowing at the network layer was detected using the mean length of error bursts for ARQ control. In [26] shadowing was detected through ARQ timeouts. Notice that even techniques combining ACM and ARQ without relay selection assisted by shadowing detection, such as in [27], could lead to network load increase by increasing the number of retransmissions.

Therefore, these detection methods based solely on SNR measurements failed in detecting shadowing events when it was raining due to two main reasons. First, these detectors used a fixed threshold that assumed a shadowing event every time a signal attenuated by rain fading reaches a level below the shadowing threshold. Second, because shadowing events are independent of the atmospheric conditions, it can happen anytime during rain, thus, even a shadowing detector with variable threshold is unable to operate properly. If shadowing could be detected during rain, mitigation techniques such as ACM could be used during a longer period of time, besides enabling other benefits regarding power and spectrum, as mentioned above. To the best of the authors knowledge, the problem of shadowing detection for LMS channels in the presence of rain at Ka-band has not been addressed and seems to be an open research question.

The shadowing detector proposed in this paper is based on Interactive Multiple Model (IMM) filter [28], [29]. The IMM filter, a well-known target tracking technique based on signal estimation based on a set of system models running in parallel Kalman filters [30], [31], was initially employed in applications such as aircraft tracking [32], GNSS navigation [33], and communications systems [34]. One major requirement of using an IMM filter is to know the collection of models that the system can reside in, which in our case translates into knowing the communications channel model. Communications channel modeling often attempts to consider all fading and noise sources. However, it is almost impossible to precisely model all weather and environmental dynamics, due to the large amount of variables that are functions of several other global scale elements. If possible, knowing the exact models would allow us to predict the channel behavior with very low error margin. As mentioned before, for a satellite channel, a precise noise model would require knowledge of every single noise source affecting the channel as well as its behavior in time, which is almost impossible to determine at the present. Some recent research papers proposed techniques to estimate these values [35]–[40]. The primary issue with these techniques is that they are mostly constrained to work under certain conditions, are designed for a specific purpose or application, and the system model is assumed to be known. An alternative approach to unknown model parameters framework is to account for them in the process noise covariance matrices based on the assumption that these unknown parameters and the channel noise are Gaussian distributed, as shown by previous numerical experiments [29], [33], [34], [41].

Regarding measurement campaigns for the LMS channel at the K-band, only a few publications in the open literature are available. Previous work has been performed with respect to LMS channel modeling using both theoretical studies and measurement campaigns for L- and C-bands that date back to 1991 [42]. However, each study targets a very specific

scenario in terms of location, building density, frequency band, and antenna elevation angle. Most of these previous works did not take into consideration the weather and its impact on the transmission performance, although several of these past works have contributed to a number of ITU recommendations, especially at L- and S-bands [15], [43]–[45]. Other researchers have investigated Global Navigation Satellite System (GNSS) receivers when deployed in LMS channels [46], [47]. Across the K-band frequency range, a general Ku-band channel model was provided in [48], while in [49] a channel model that considers tropospheric scintillation effects at Ku-band was presented. In [16] a theoretical performance study that considers the effects of rain fading on the LMS channel at Ka-band frequencies was presented.

Other measurement campaigns focused on rain fading, such as NASA's ACTS and OLYMPUS programs [50]–[52], and a consortium of five European countries that used the commercial satellite Alphasat to conduct propagation measurement campaigns across Europe [53], all have measured rain attenuation at Ka-band as well as other atmospheric effects. Ka-band measurement campaigns using purely experimental satellites have also been reported, such as Fedsat [54] from Australia, WINDS from Japan [55], and Hotbird 6 from France [56]. Data from these activities tend to be available only to the research group conducting the experiments. We recognize that simple statistical models (some of which were obtained using data from these aforementioned measurement campaigns), such as those described by several International Telecommunications Union (ITU) standards [57], [58] have been used for years by satellite designers in order to perform transmission performance analysis, and attenuation time-series were never a requirement for the development of satellite link-budgets. However, to the best of the authors' knowledge, given that none of this data is publicly available, the only way to provide rain attenuation time series data to a Ka-band satellite channel simulator is to use synthesized time series based on the ITU recommendations.

The main objective of this paper is to propose a real-time shadowing detector algorithm for satellite receivers operating on LMS channels at Ka-band during rain, with a small false alarm detection rate when the terminal is fixed or not experiencing signal shadowing. Analyses are conducted considering a downlink between a mobile terminal and a GEO satellite, as illustrated in Fig. 1, with the terminal experiencing five different channels: LOS during rain (fixed terminal), suburban LMS during clear sky and rain, and rural LMS during clear sky and rain. To achieve this objective, several challenges are considered, namely:

- Design of a shadowing detector for mobile terminals capable of detecting shadowing on LMS channels during clear sky and rain,
- Acquisition of satellite signal measurement time series for different channels while operating under different weather conditions, and
- Accurate channel modeling for each scenario.

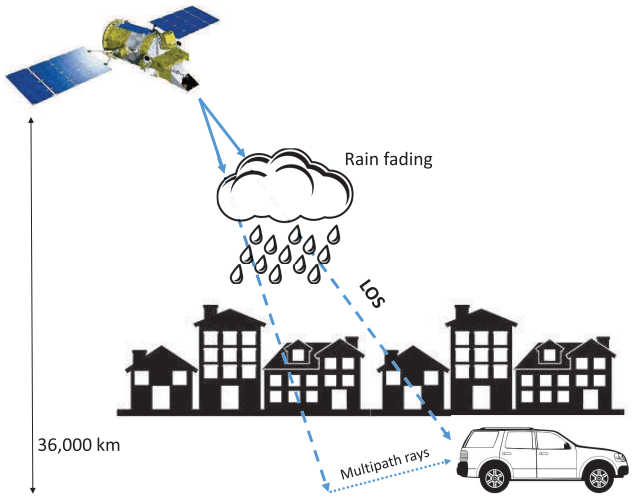

FIGURE 1. Illustration of a GEO satellite communicating via a Ka-band land mobile satellite channel to a mobile ground node during rain fading. The received signal is a combination of both LOS and shadowed multipath faded signals.

In order to address the issues mentioned above, the main contributions of this paper are the following:

- A novel IMM filter-based shadowing detector algorithm for operation through GEO satellite link at Ka-band for fixed and mobile terminals during rain,
- An automatic search algorithm for a system's process noise covariance matrix for IMM filters, and
- A detailed algorithm implementation of the time series generators of rain attenuation and LMS channel with variable sample rate, based on updated ITU recommendations from 2013 and 2015.[1]

In addition to these contributions, the performance of the proposed shadowing detector algorithm is compared against some current state-of-the-art detector schemes.

The rest of this paper is organized as follows: Section II gives an overview of satellite communication time series generation for Ka-band when operating in clear sky and rain fading conditions. Section III presents the proposed IMM filter design. Section IV presents the simulation results of the time series synthesizers, as well as the IMM filter together with the events detection. Section V concludes the paper and provides insights about future work.

II. Ka-BAND SATELLITE COMMUNICATIONS CHANNEL EXPERIENCING RAIN FADING

There is increasing demand for satellite communication systems operating over the Ka-band due to its spectral availability. However, this frequency band is susceptible to several atmospheric impairments that play a key role in determining the performance of the satellite communication link. The main source of attenuation in this band is rain, which is responsible for the effects of slow fading caused by the energy absorption of electric fields traveling across water molecules at certain frequencies. Signal attenuation is also caused by

[1] Available on GitHub [59]

other atmospheric effects such as wind speed, cloud density, and gases such as oxygen and water vapor [57], [60], [61].

Each of these attenuation sources is a function of not only the frequency band but also the elevation angle, geographical location, and the time of day and year. These conditions result in design challenges that vary spatially and over time. Consequently, SDR can help resolve these issues and provide flexible and adaptive solutions due to its reconfigurable attributes in real-time. Thus, devising algorithms capable of tracking the current channel condition and informing the radio platforms about the appropriate transmission/reception configuration that yields the overall optimum performance in terms of bit error rate (BER), will help robust satellite communication systems operating in the Ka-band to be achieved.

In addition to atmospheric impairments, the total attenuation is also a function of the satellite orbit, as well as the ground station mode. A GEO orbit is considered in this paper, where the satellite possesses a fixed location in the sky with respect to a user on Earth at a distance of 36, 000 km from the Equator. The ground station can possess both a fixed or mobile location; we consider both scenarios in this paper. Satellite communication links operating across the Ka-band and experiencing rain attenuation are considered in this work.

A. RAIN ATTENUATION TIME SERIES SYNTHESIZER AT Ka-BAND

Due to the lack of available measurement data, especially of rain fading impairments at Ka-band, attenuation time series had to be synthesized based on the recently updated ITU recommendations. In order to generate the synthetic rain attenuation levels, a method proposed by ITU-R P.1853-1 [62] was employed, where three inputs were required: (i) Complementary Cumulative Distributive Function (CCDF) of rainfall rate for the desired location; (ii) the percentage probability of rain in an average year, $P0$, for the desired location; (iii) the attenuation levels exceeded in decibels for the percentages of time used to compute the CCDF. Although it is known that cumulative statistics as well as rain attenuation dynamics depend on the relative motion speed between the mobile user and the advection of rain cells due to wind, the analysis and results provided by this work assume wind speed equal to zero, and future work is expected to consider the other atmospheric effects mentioned above, including rain cell advection due to wind speed. In this work, the following time percentages were used:

$$[0.01, 0.02, 0.03, 0.05, 0.1, 0.2, 0.3, 0.5, 1, 2, 3, 5, 10]. \quad (1)$$

$P0$ represents the probability of rain at the GS in an average year and can be estimated based on information derived from 40 years of data from the European Centre of Medium-range Weather Forecast (ECMWF) [60] or from local measured rainfall rate data. This probability value $P0$ is required to compute the probability of rain attenuation on the slant path. Using the ITU-R P.837-6 [60] and focusing on the location of Worcester, MA, USA (lat 42° 16′ 30.8″ N, lon 71° 48′ 25.2″ W), a CCDF for rain rate and $P0$ were computed. Then, the rain rate values from the CCDF were converted into attenuation levels (dB) using the specific attenuation equations from ITU P.618-12 [57] specifications using parameters given by ITU P.839-4 [63], such as the rain height, as well as parameters given by ITU-R P.838-3 [61], such as the circular polarization for a carrier frequency f_c at 26 GHz. Finally, using the method proposed by ITU-R P.1853 [62], a rain attenuation time series was generated, which assumed an elevation angle of 34°, at a sampling rate of 1 Hz across a time period of 84, 600 seconds. A snapshot of 512 seconds of a generated times series is shown in Fig. 2, which is the same time series used in other scenarios, further described in later sections.

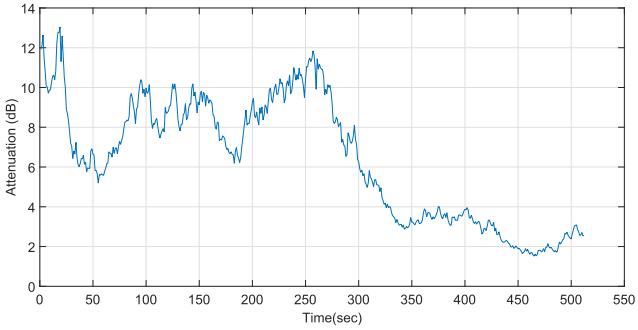

FIGURE 2. Rain attenuation time series for Ka-band based on ITU-R P.1853. Note that during the entire time interval the channel is facing rain fading.

1) LMSS CHANNEL SIMULATION AT Ka-BAND

Given the ground station mobility, the Earth-space land-mobile satellite service (LMSS) channel time series was generated based on ITU-R P.681-8 [58] communicating across the Ka-band with a GEO satellite. For a more realistic propagation simulation, both statistical and stochastic models for mixed propagation conditions, such as rural, wooded, urban, and suburban areas, were also employed. This model computes the cumulative distribution function (CDF) using a semi-Markov 2-state model represented by a non-shadowed (good) state and a shadowed (bad) state, where the state duration follows a log-normal distribution and the signal within each state follows a Loo distribution. The log-normal shadowing affects only the direct component, while the diffuse multipath components have a constant average power [64].

It is worth noting that the ITU-R P.681-8 version used in this paper recommends the usage of parameters measured specifically for a suburban area at 11.7 GHz rated to be used by any frequency between 10 GHz and 30 GHz, thus covering the lower portion of the Ka-band. The ground vehicle speed v_m was set to 33 km/h, while the elevation angle was set to 34°. Furthermore, the angle between the vehicle heading vector projected on the ground and the satellite azimuth vector projected on the ground was specified to be equal

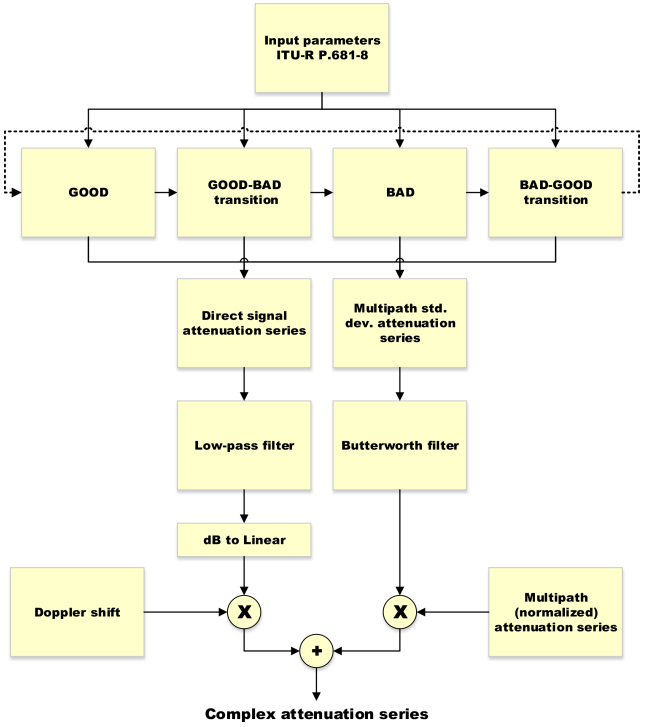

FIGURE 3. LMS channel simulator diagram block based on ITU-R P.681-8. After good/bad state time series generation, the same input parameters are provided to the state attenuation time series synthesizers, including good, bad and their transitions. Matlab code implementation provided in [59].

to 0°. The sampling frequency f_s was assumed to be equal to 10, 000 samples per second, which is a function of the carrier frequency f_c, as well as of the maximum speed of the vehicle v_{max}, given by [65]:

$$v_{max} \leq \frac{c_0 f_s}{2 f_c}, \tag{2}$$

where c_0 is the speed of light. The synthesizer diagram block, shown in Fig. 3, was implemented in MATLAB (source code available in [59]). Instead of the recommended Jakes model, a 10^{th}-order low-pass Butterworth filter with normalized 3 dB cutoff frequency equal to:

$$f_c = \frac{f_{Doppler}}{f_s/2}, \tag{3}$$

was used to reproduce the fast variations due to multipath since it is more realistic for an LMS channel than the Jakes model [15]. Note that $f_{Doppler} = \frac{v_m f_c}{c_0}$ is the maximum Doppler frequency. The time series was generated as follows: Using the input parameters provided by the ITU-R P.681-8, parameters are generated for the two states as well as for the transitions between them (for implementation purposes, transitions are considered states too). Then, a complex time series for both direct and multipath components were generated. Since the direct signal suffers from slow fading, it is filtered by a low-pass filter with transfer function:

$$H(Z) = \frac{\sqrt{1-\rho^2}}{1-\rho Z^{-1}}, \tag{4}$$

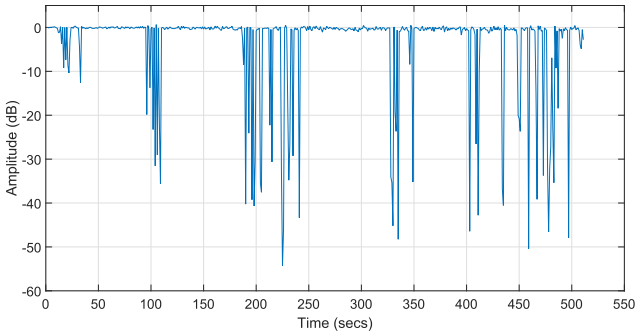

FIGURE 4. Example of an LMS channel synthetic attenuation time series at Ka-band based on ITU-R P.681-8. Shadowing due to mobile terminal LOS blockage by buildings and trees are represented by deep attenuation values, where the good and bad states are Loo distributed.

where:

$$\rho = exp\left(\frac{-v_m\,(1/f_s)}{L_{corr}}\right), \tag{5}$$

and L_{corr} is the correlation distance given by [58]. The phase of direct signal is defined by the maximum Doppler frequency, while the multipath series is filtered using the Butterworth filter. Note that the synthesizer implementation employed in this paper differs from that found in [15] since the latter uses a maximum transition rate (shadowing slope) of 5 dB/m while the former uses the recommended linear interpolation of the parameters during all transitions between good (bad) and bad (good) states. This leads to a more natural transition of the mean and standard deviations of the Gaussian random variables used to generate the raw series for both direct and multipath signals.

The implementation employed in this paper generates data at a sampling rate of f_s, resulting in a total of 5.12 million samples. However, to comply with the rain attenuation time series, the LMS synthesizer output is down-sampled to 512 samples, as shown in Fig. 4.

For the scenario where we have a mobile LMS channel during a rain fading event, we add together the previous two time series. A step-by-step block diagram for the algorithm of the complete fading time series generator is provided in Fig. 5. The resultant attenuation time series is shown in Fig. 6. Several aspects that differ between the analysis proposed in this paper and those found in [16] included the following: (i) in this paper we consider the power attenuation over both direct and multipath signals for both shadowed and non-shadowed scenarios; and (ii) this paper uses synthesized time series based on the updated ITU recommendations, with the goal of analyzing the attenuation values on a per second basis rather than an annual shortage percentage. However, both studies assume that the rain possesses minimal influence on the probability density function (PDF) with respect to shadowing events in clear sky scenarios. Consequently, the shadowing resulting from both direct and multipath rays, as well as the rain attenuation from these same direct and multipath rays, can be considered to be two independent stochastic processes.

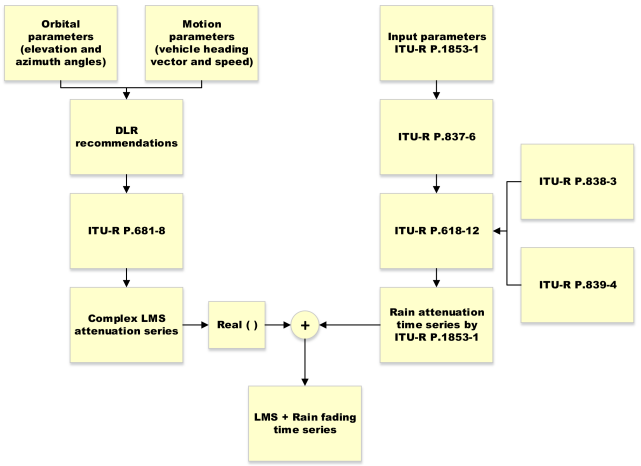

FIGURE 5. Block diagram of complete attenuation time series generator algorithm. Output time series is a combination of the individual rain fading time series and the LMS channel time series, generated individually.

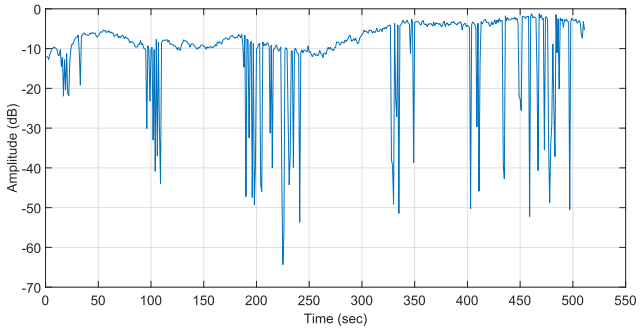

FIGURE 6. LMS channel time series during rain fading for a constant speed mobile ground receiver communicating with a GEO satellite at Ka-band.

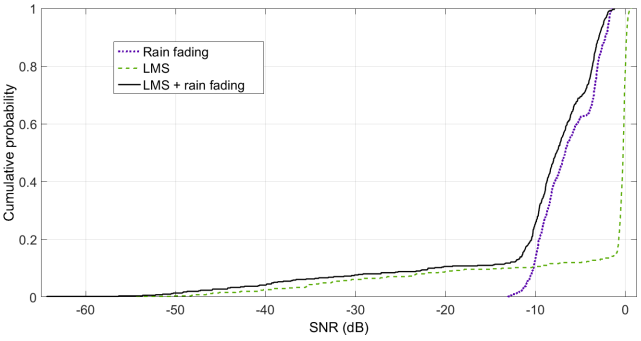

FIGURE 7. Addition of rain fading to the LMS amplitude. Notice the change of the mean in the PDF. As expected, both events are independent.

When comparing the cumulative distribution function (CDF) of the LMS channel time series (shown in Fig. 4) with the CDF of the same LMS time series but with the effects of rain attenuation at Ka-band included (shown in Fig. 2), we observe that the resultant channel possesses a log-normal PDF since only the mean of the LMS PDF changes, which is observed in Fig. 7. Thus, it can be deduced that an LMS channel experiencing from rain fading possesses a smaller mean.

III. PROPOSED INTERACTIVE MULTIPLE MODEL (IMM) USING KALMAN FILTERS

In order to perform shadowing detection in the presence of rain, a signal state classification is proposed to be done by a filter that is capable of state estimation in the presence of noisy measurements such as the Kalman filter. The Kalman filter, fully explained in [66], estimates a signal contaminated by two noise sources, process noise $w(k)$ and measurement noise $v(k)$, respectively, using the state space equations without control, namely:

$$X(k+1) = F \cdot X(k) + w(k), \tag{6}$$

which is responsible for modeling the state evolution, while

$$z(k) = H \cdot X(k) + v(k) \tag{7}$$

describes the noisy outputs of the measurement sensor. In our case, the transition matrix F in Eq. (6) is expressed as:

$$F = \begin{bmatrix} 1 & dt \end{bmatrix}, \tag{8}$$

which is a time-invariant constant velocity model that allows for the projection of the current estimated state, in our case the measured power k-steps ahead, controlled by dt assumed to be equal to 1. Note that, the rest of this paper refers to the synthetic time series that is output from the simulator as the 'original' time series, and to the time series affected by sensor noise as the 'measured' time series. The observable state $z(k)$ is the measured received power amplitude, thus, $H = 1$. The process noise $w(k)$ and the measurement noise $v(k)$ are both zero-mean Gaussian distributed with covariance matrices Q and R, respectively.

The first step in setting up a Kalman filter is to have an accurate system model that describes the majority of different system behaviors. For instance, several specific behaviors can be modeled when tracking a target position for navigation purposes, such as the speed and acceleration of an aircraft [32], [40], [41], [67]. In these cases, the model fully describes the system dynamics, with few uncertainties left to the noise functions $w(k)$ and $v(k)$.

For the model being addressed by this paper, namely, the atmospheric environment, we would like to include as many local weather variables in the model as possible, such as the influence of the current tropospheric temperature, wind speed, amount of clouds in the area, and all the time evolutionary behavior of each of these variables. However, such modeling is known to be very complex, thus developing both a state space model and a transition matrix that accounts for the effects of all these variables and their evolution over time is considered to be outside the scope of this work. Nevertheless, based on the assumption that these unknowns have the same Gaussian distribution as the noise [29], [33], [34], [41], our proposed approach uses a very simple state space model which accounts for the uncertainties in the process noise $w(k)$, which ends up into estimating parameters such as covariance matrices, described in the following subsection.

The Kalman filter approach used in this work can be summarized by the following equations, which can be further

divided into two sets of equations. The first set is responsible for predictions of $\hat{X}_j$, given by:

$$\hat{X}_j(k+1 \mid k) = F \cdot \hat{X}_{j0}(k \mid k), \tag{9}$$

with the covariance P_j given by:

$$P_j(k+1 \mid k) = F \cdot P_{j0}(k \mid k) \cdot F^T + Q. \tag{10}$$

The second set performs updates of the Kalman gain K_j:

$$K_j(k+1) = P_j(k+1 \mid k) \cdot H_j^T \cdot (S_j(k+1))^{-1}, \tag{11}$$

where the residual covariance matrix S is computed by:

$$S_j(k+1) = H \cdot P_j(k+1 \mid k) \cdot H_j^T + R_j. \tag{12}$$

$\hat{X}_j$ and P_j are updated using the expressions:

$$\hat{X}_j(k+1 \mid k+1) = \hat{X}_j(k+1 \mid k) + K_j(k+1) \cdot e_j(k+1), \tag{13}$$

$$P_j(k+1 \mid k+1) = P_j(k+1 \mid k) - K_j(k+1) \cdot S_j(k+1) \cdot K_j^T(k+1), \tag{14}$$

where the residual e is computed using the expression:

$$e_j(k+1) = z(k+1) - H \cdot \hat{X}_j(k+1 \mid k). \tag{15}$$

Since in our case the conditions for an optimal Kalman filter are not satisfied (if known, a realistic model of atmospheric impairments affecting the communications channel would be non-linear), an extended version known as IMM filter has been proposed in order to perform recursive estimation when continuous uncertainties Gaussian distributed, such as additive white Gaussian noise (AWGN), and discrete uncertainties such as finite system states, are assumed [29], [33], [34], [41]. The IMM filter is composed of a finite number of Kalman filters, and each filter is designed to represent a different system behavior, or state.

Each Kalman filter input $\hat{X}_{j0}$ is computed by [29]:

$$\hat{X}_{j0}(k \mid k) = \sum_{i=1}^{N} \hat{X}_i(k \mid k) \mu_{i,j}(k), \tag{16}$$

for $i, j = 1, 2, \cdots, N$ used to identify the Kalman filters within the IMM filter ($_{j0}$ refers to IMM mixed values only). The mixing probabilities $\mu_{i,j}$ at instant k are computed by:

$$\mu_{i,j}(k) = \frac{\pi(i,j)\mu_i(k)}{\hat{\mu}_j(k+1 \mid k)}, \tag{17}$$

and mixes the original Kalman filter inputs $\hat{X}_i$ with each other. The predicted model probability $\hat{\mu}_j$ from instant k to $k+1$ is computed by:

$$\hat{\mu}_j(k+1 \mid k) = \sum_{i=1}^{N} \pi(i,j)\mu_i(k), \tag{18}$$

where $\pi(i,j)$ is the Markovian state transition probability matrix [34].

The next step is to use the standard Kalman filter equations in each parallel filter, with its respective mixed inputs computed by Eqs. (16) and (19). Each Kalman filter in parallel has the same update and prediction equations presented in Eqs. (9)-(15), with the only difference being their respective Q matrices, which in our case are computed automatically, and the covariance matrices P_{j0} computed by:

$$P_{j0}(k \mid k) = \sum_{i=1}^{N} [P_i(k \mid k) + (\hat{x}_{j0}(k \mid k) - \hat{x}_i(k \mid k)) \cdot (\hat{x}_{j0}(k \mid k) - \hat{x}_i(k \mid k))^T] \mu_{ij}(k). \tag{19}$$

Finally, the individual Kalman filter estimates are combined into one IMM filter estimate using the expression:

$$\hat{X}(k+1 \mid k+1) = \sum_{j=1}^{N} \hat{X}_j(k+1 \mid k+1) \mu_j(k+1), \tag{20}$$

where the model probabilities μ_j are updated by using the expression:

$$\mu_j(k+1) = \frac{\hat{\mu}_j(k+1 \mid k) \cdot L_j(k+1)}{\sum_{j=1}^{N} \hat{\mu}_j(k+1 \mid k) L_j(k+1)}. \tag{21}$$

The likelihood function L_j is given by:

$$L_j(k+1) = \frac{\exp\left(-\frac{1}{2} e_j^T(k+1) \cdot S_j^{-1} \cdot e_j(k+1)\right)}{\left(|2\pi S_j(k+1)|\right)}, \tag{22}$$

for $j = 1, \cdots, N$. The process repeats itself for the next iteration, when a new set of measurements is acquired from the sensors.

In order to initiate the proposed algorithm the following assumptions are made: $X(0)$ is equal to the received power level under clear sky conditions; $P = [10000]$ since the covariances are expected to converge to a constant value; initial state probabilities $\mu = [0.5; 0.5]$; and the Markovian state transition probabilities are assumed to be:

$$\pi = \begin{bmatrix} 0.9 & 0.1 \\ 0.1 & 0.9 \end{bmatrix}. \tag{23}$$

In this case, π was chosen to represent the behavior of the system staying at a certain state with a higher probability than the probability of transitioning to another state. This behavior was considered based on the slow fading characteristic of the rain attenuation effect and on the deep fading characteristic of shadowing in LMS channels. In the following subsection, a more detailed explanation regarding the choice of the filter number present on the IMM filter is provided in the following subsection.

During online operations, after choosing the Q matrices, at each iteration one SNR measurement is input and two output probability values, computed by Eq. (21), from each Kalman filter inside the IMM filter, are compared against a threshold. Fig. 10 presents the state decision output for a threshold value equal to 0:5.

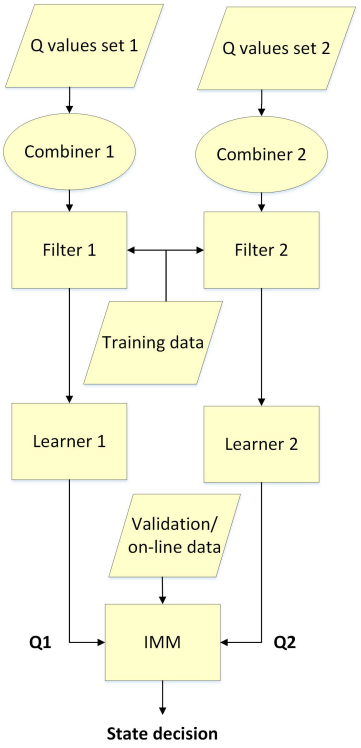

FIGURE 8. Diagram block for the proposed design for search of Q matrix integrated with the IMM filter design. Each matrix combination is tested individually. Q1 and Q2 are the output matrices chosen by the learning blocks. The ultimate IMM output is the state decision if there is shadowing or not.

A. DEFINING NUMBER OF FILTERS IN IMM

When designing an IMM filter, one of the key requirements is to define how many Kalman filters should be used. Each Kalman filter in an IMM filter is often used to model one system state [29], [41], [67], and the IMM filter computes probabilities to most accurately identify which model reflects the system current behavior. Thus, one must know beforehand which system behaviors will be tracked by the IMM filter, such that a Kalman filter can be designed for each of them. In this paper, we used two filters that model the detection of shadowing in LMS channels, being able to distinguish deep fading from slow fading, such as due to rain attenuation. The primary idea here is to have one filter that quickly follows the noisy SNR measurements steep transitions caused by shadowing, and the other filter to follow the slower transitions caused by rain fading.

B. AUTOMATIC SEARCH FOR Q

In the previous section, the problem of modeling the system was left to defining values for the R and Q matrices, which represent the measurement and noise process noise variances based on the assumption that these noise sources are Gaussian. Since R is an independently generated value of the system relative to our measurements, we can assume R to account for only the noise resulting from the sensor. Thus, R is assumed to be known, and can be measured offline using a known input.

Considering the primary goal of allowing the system to estimate measurements from noisy inputs, the cost function to be minimized is the mean-squared error (MSE). In order to achieve this goal, an approach that tests and builds the different Q matrices for each parallel Kalman filter is proposed as shown in Fig. 8, which illustrates their diagram blocks, and by Algorithm 1, which describes the step-by-step usage of the proposed model for shadowing detection.

The algorithm is initiated with different sets of possible variance values for each parallel Kalman filter. In order to tailor each parallel filter to a different behavior, or mode, one needs to provide different ranges of values for each set, through which the search algorithm will look for and build the Q matrices. One of the goals of this paper is to demonstrate and analyze the IMM performance using a simple model that distinguishes between attenuation slopes, with slower changes being a characteristic of clear sky or rain conditions, and very steep slopes being a signature of shadowing events. Thus, only two different modes, *i.e.*, two different Q matrices, are necessary: (i) a mode with small values indicating slower attenuation slopes, and (ii) a mode with large values indicating steeper attenuation slopes. This idea is standard for IMM filter designers, in which there is one model and two filters representing the system state being or not in that model. In the literature [29], [31], [67], values used to distinguish states in various model approximations, such as aircraft tracking, are two to three orders of magnitude apart. Further details are described in Section IV of this paper.

Given that both filter models run in parallel within the IMM, the output of each iteration is a combination of both operations depending on their respective probabilities to distinguish between no fading and/or slow fading, and deep fading modes. As a result, the technical challenge associated with this operation is identifying the correct mode, or at least the most probable one at each instant.

While designing these filters, it was noted that large values in a Q matrix make the IMM filter rely more on its noisy inputs, thus its output follows the noisy inputs more closely. Furthermore, this choice of Q causes the output to quickly change its values in an attempt to follow the rapidly changing input, such as when noise or deep fading is present. On the other hand, for small values of Q the output of the IMM slowly follows the changes in the inputs. Thus, the result is an smoothed output with respect to its input. Each Kalman filter attempts to track the signal within the noise, thus when the IMM mixes their output probabilities, it makes easier to distinguish deep fading from noise and slow fading, allowing for the detection of shadowing events even in the presence of rain.

It is worth noting that when building Q matrices by combining the values available in a set, for the Kalman filtering equations to be computed properly one needs to make sure that Q must be symmetric and all of its eigenvalues must be positive, *i.e.*, Q must be positive definite since it needs to be invertible. In the following section, we discuss the

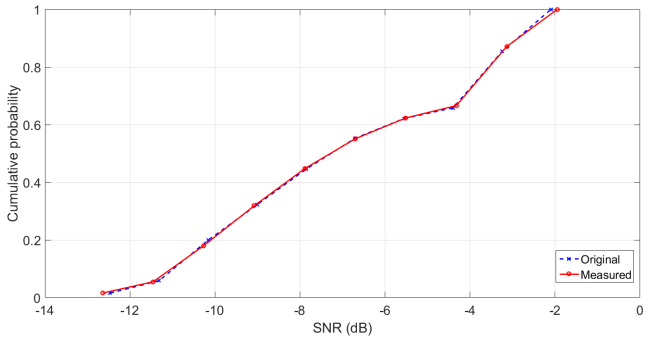

FIGURE 9. Normalized CDF of LMS channel time series during rain fading, shown in Fig.6 (Original) and its CDF after measurement by noisy sensor (Measured) for R=0.1.

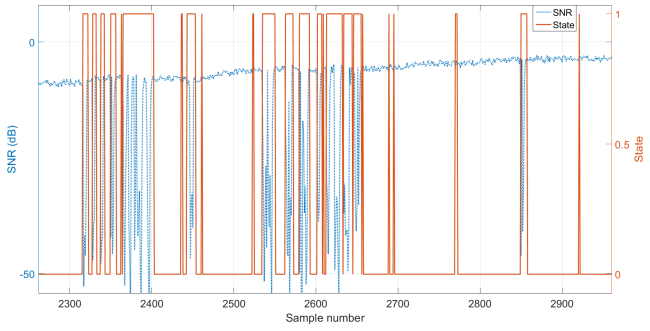

FIGURE 10. IMM outputs of state detection for mobile terminal using a Ka-band link with a GEO during rain fading through an suburban LMS channel. The measured received amplitude values and its respective states are shown for comparison. Shadowing detection is achieved at different levels of attenuation due to rain fading. Samples recorded at 10Hz.

performance of the proposed IMM approach for each of the scenarios mentioned in the previous section.

For each set of values, Q matrices are constructed by evaluating all possible combinations of these values within the Q matrix. The process occurs in parallel and iteratively for all Kalman filters until all the possible Q matrices are evaluated. In Fig. 8, this parallel process is depicted by the 'Combiner 1' and 'Combiner 2' blocks.

The outputs of each 'Combiner' are used by the individual Kalman filters using only Eqs. (9)-(15). The filters are operated using a training dataset and the MSE of the outputs from each individual filter is recorded. Then, each individual 'Learner' independently decides which Q matrix met a certain requirement, in this case, the minimum MSE. The result of each 'Learner' is then fed into the main IMM, for validation and online estimations. Comments about its performance evaluation are given in Section IV.

This proposed methodology allows the system to update its Q matrices in order to operate under changing environments for achieving a better performance. The determination of how frequently Q should be re-evaluated is currently under investigation by the authors, and is outside the scope of this work.

Algorithm 1 Proposed Shadowing Detector Operational Routine

Require: Initial parameters

```
Define training window size n
Select number of states to be detected s
Choose s sets of Q-values of any size within different ranges each
Define s − 1 thresholds values for state detection
Build all possible c_s combinations of matrices for each of the s sets
Choose optimization metric
for t = 1:end of operation do
    if t > n then
        Receive new measurement z
        for k = 1 : 1 : s do
            for j = 1 : 1 : c_s do
                Train individual Kalman filters
                Learn Q-matrices for optimized chosen metric
                Run IMM filter
                Get detected state value
            end for
        end for
    else
        Update training window
    end if
end for
```

IV. SIMULATION RESULTS

In this section, the proposed IMM filter performance is analyzed for five different channel conditions: (i) fixed receiver under rain, (ii) LMS rural under clear sky, (iii) LMS rural under rain, (iv) LMS suburban under clear sky, and (v) LMS suburban under rain. The input to the IMM filter is the time series of synthesized noisy SNR measurements at the receiver. For simulation purposes, the noise measurement process is assumed to be Gaussian with zero mean and standard deviation R with values equal to 0.1, 0.5 and 1. The search for the Q matrices Q1 and Q2 was performed building matrices using all combinations of values from two independent sets. The set for Filter 1 is: $[0,\ 10^{-10},\ 10^{-3}]$, and for Filter 2 is: $[10^{-10},\ 10^{-1},\ 1,\ 10]$. The careful reader might note that included in the ranges are 0 and 10^{-10}, which are very close to each other, indeed our results show that there is a difference in performance when choosing one over the other. Notice that the sets used contain different amount of values, since there is no requirement regarding the maximum number of elements of each set. However, an increase in the number of elements increases the total number of combinations that must be tested during training of the Kalman filter. The IMM proposed approach was tested using the MSE of the SNR estimations, the same metric used for the automatic search of Q matrices during training.

Considering the time series length, the IMM filter performance was evaluated using three different training dataset

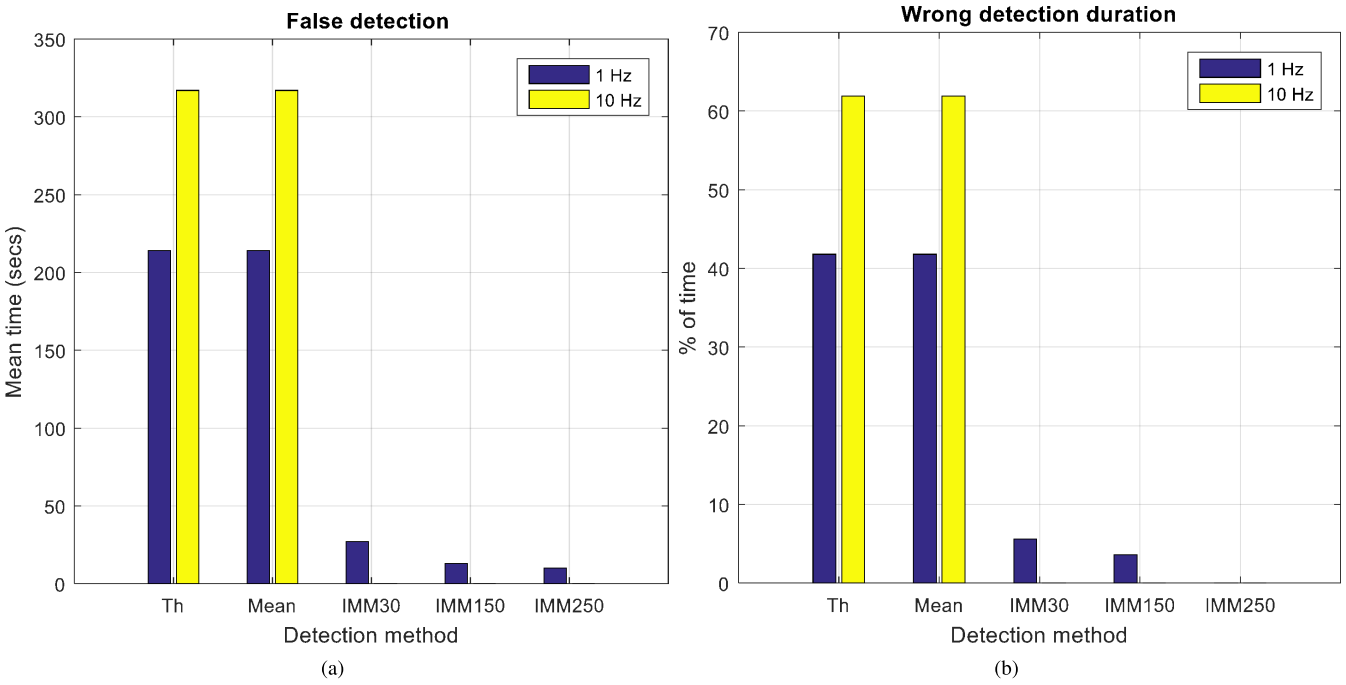

FIGURE 11. Shadowing detection performance in scenario with rain fading and no shadowing, for a fixed terminal using a Ka-band link with a GEO satellite. Average duration of false shadowing detection (a) when no detection is expected, and its corresponding percentage of total simulation time doing wrong shadowing decisions (b). Lower false detection mean time duration is better. Both threshold SNR and mean SNR methods show poor performance.

TABLE 1. IMM filter MSE of rain faded channel - 100 runs.

	R= 0.1		
Training dataset size	50 samples	150 samples	250 samples
Mean	33.99	26.66	17.22
Std. dev	0.9	0.79	0.56
	R= 0.5		
Training dataset size	50 samples	150 samples	250 samples
Mean	31.87	25.95	19.41
Std. dev	1.95	1.78	1.58
	R= 1		
Training dataset size	50 samples	150 samples	250 samples
Mean	10.02	8.05	5.85
Std. dev	1.64	1.39	1.22

sizes, with the largest one being half of the time series duration. After the Q1 and Q2 matrices were chosen, the testing dataset was used to validate the performance of the IMM filter. Table 1 shows the validation MSE statistics for 100 simulation runs for three different R values for a scenario with a fixed terminal experiencing rain fading only, and for the three different training dataset sizes. Despite the smallest mean error values for the measurement standard deviation $R = 1$, the mean error for $R = 0.1$ and $R = 0.5$ can be considered similar, with $R = 0.1$ presenting the smallest standard deviation error values, as expected. Also, for all different values of R, the mean error linearly decreased with the increase of the training dataset size, as expected. Since R is a parameter directly related to the hardware being used, it is out of the scope of this paper to discuss better approaches to improve the IMM performance function of R values. Thus, the rest of this paper assumes $R = 0.1$, and as shown by Fig. 9, the normalized CDF of both original attenuation time-series and measured time-series considering the noisy sensor with $R = 0.1$ are very similar. For the five scenarios mentioned above, the Q values for the IMM inner filters 1 and 2, were computed, respectively, as:

$$Q1 = \begin{bmatrix} 10^{-3} & 0 \\ 0 & 10^{-3} \end{bmatrix}, \tag{24}$$

$$Q2 = \begin{bmatrix} 10 & 10^{-10} \\ 10^{-10} & 10^{-10} \end{bmatrix}. \tag{25}$$

For $Q1$, the algorithm preferred the value of 10^{-10} over 0 for the variance value of the rate. This shows that a very small change of values had an impact on the decision of the final Q matrix, indicating the level of sensibility that the automatic Q search method provides.

Tracking the inner filter probabilities values μ indicates which filter has a higher probability of having a model that best describes the current environment behavior, defined in this paper as the channel states. Using a threshold of 0.5 the IMM inner filters 1 and 2 represent the states 0 and 1, no shadowing and shadowing states, respectively. For instance, during the deep fading events, IMM filter outputs higher than the threshold probability values for Filter 2, leads to the detection of State 1 indicating shadowing is being experienced by the signal. Fig. 10 illustrates a snippet of the state decision time series output together with the measured SNR at the receiver. Several shadowing events were detected at different attenuation levels, in this case solely due to rain fading.

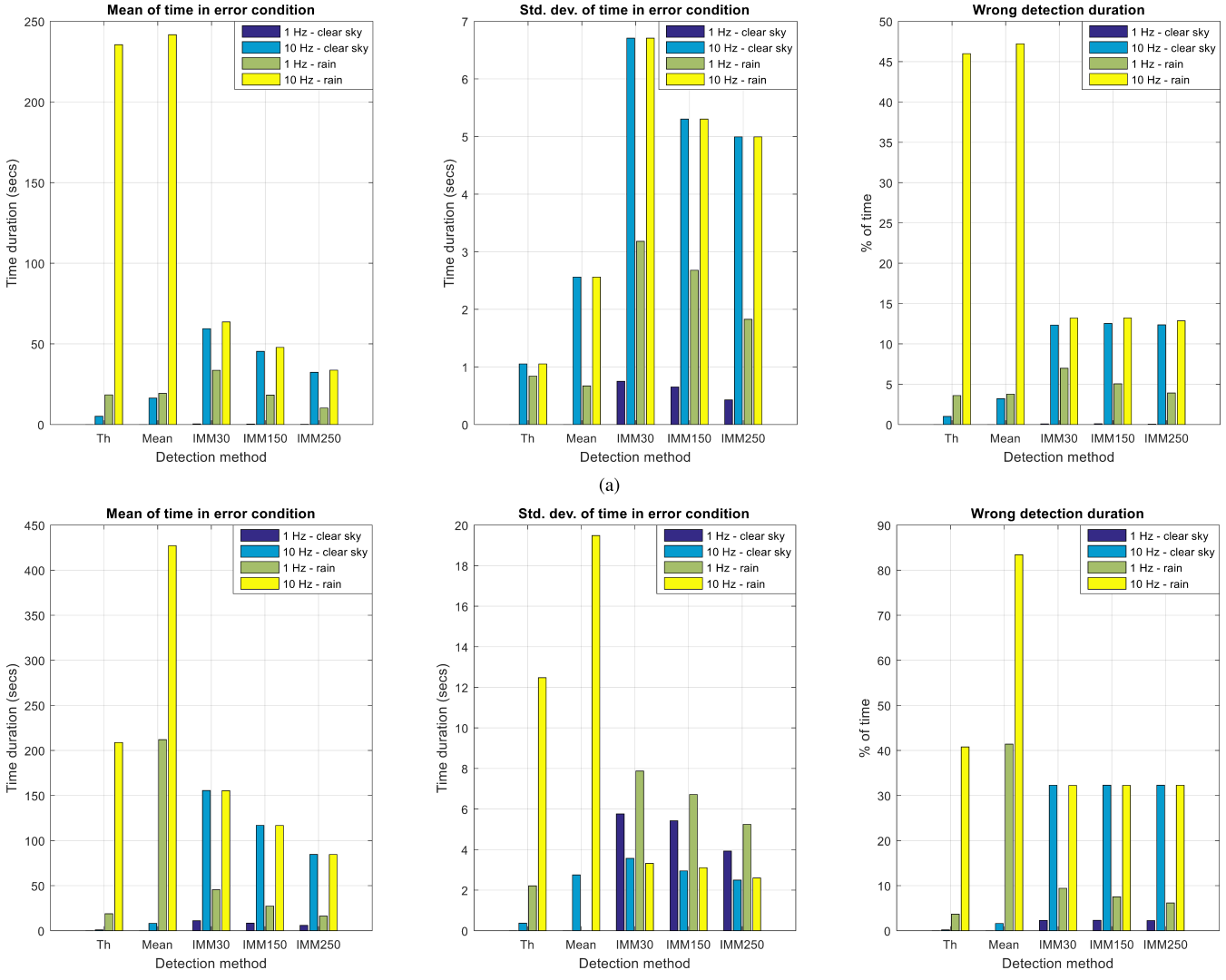

FIGURE 12. **Shadowing detection performance on suburban (a) and rural (b) LMS channels during clear sky and rain conditions. Lower time duration means better performance. Shadowing detection on LMS channels by IMM filter is invariant to atmospheric conditions when sampled at 10 Hz, and better performance was achieved during rain by spending less time in erroneous shadowing detection condition when compared to current state-of-the-art detectors.**

Notice that the detection is not ideal and a few samples caused false alarm detection. These errors are believed to be related to IMM filter prediction errors for only a few samples, and further investigation is required to fully understand the reason of this error. Since signal shadowing occurs in a sequence of samples, single detections can be ignored by the algorithm making use of this detector. Furthermore, it is worth noting that the dominance of one of the filters occurs based upon the current channel shadowing conditions and how each filter was designed, independently of the fading. This is implied within the order of magnitude difference among the values available for the initial set that each Q matrix is constructed from.

In order to assess the performance of the proposed shadowing detector through different scenarios and to compare our proposed approach with some common state-of-the-art detection methods, simulations were conducted for five different scenarios, described above. Each scenario was sampled at two different rates, 1 Hz and 10 Hz, 100 times with 512 seconds duration each, resulting in more than 14 hours of synthesized attenuation time series, containing only rain, shadowing, or a combination of these two impairment sources. Note that the 100 different time series for a certain scenario was simulated to get the statistical performance of the randomness of the communication channel, using the same original attenuation time series. For each scenario, 5 detection methods were compared: SNR threshold, mean SNR, and the proposed IMM with three different training dataset sizes (30, 150, and 250 samples).

Since the shadowing events were simulated, the ideal detection time series are known beforehand and were used as a baseline for comparison against the detector outputs.

Statistical shadowing detection performance was assessed on three major categories, over the time slices: mean time duration of wrong detection, standard deviation of wrong detection, and percentage of total time of wrong detection. Fig. 11 shows the detection performance in a scenario with a fixed terminal experiencing only rain fading, without shadowing, allowing evaluation of false detection performance. Both threshold SNR and mean SNR detection methods showed poor performance with more than 60% of the time making false detection at a sample rate of 10 Hz. However, the IMM filter showed a very good performance with close to zero false detection. These results motivated the majority of the research present on this paper to be extended to several different LMS channels, under different atmospheric conditions.

Regarding the sample rate, we present a comparison between 1 Hz and 10 Hz results in order to show to the reader the impact of choosing a different sample rate value to track a certain channel phenomena, as well as to illustrate its potential to be used within similar scenarios but with different purposes of state tracking. The remaining performance evaluation discussion considers only the 10 Hz sample rate, since it is the most appropriate to capture the shadowing effects based on the minimum time-series sample rate for a mobile terminal, as mentioned in [65].

On suburban scenarios, shadowing detection was evaluated under clear sky and rain conditions. The results, illustrated in Fig. 12, show that the IMM filter behavior in terms of mean time duration of detection error and total percentage of time doing wrong detection is similar and immune to the presence of rain. However, the performance of the other methods, SNR threshold and mean SNR, will vary substantially depending on the channel atmospheric conditions. These possess a relative good performance during clear sky conditions, even somewhat better than the proposed IMM filter, but an extremely poor performance during rain with a difference of more than 32% in this case for the percentage of total time duration doing wrong decisions.

Simulations were performed for rural scenarios as well, for both clear sky and rain conditions. The results shown in Fig. 12 also confirm that the proposed IMM filter method has a better performance for shadowing detection during rain on LMS channels in rural scenarios, where a minimum of 8.5% improvement on percentage of time duration of wrong detection was achieved by the IMM filter over the SNR threshold method. As in the suburban scenario, the IMM filter performance during clear sky and rain conditions was similar. The SNR threshold and mean SNR showed a better performance during clear sky conditions with very low mean time duration of detection error and percentage of time duration.

V. CONCLUSIONS

Using synthesized attenuation time series for five different GEO satellite channels experiencing clear sky and rain conditions, this paper presented simulation results on the advantages of using the IMM filter for shadowing detection for fixed and mobile terminals during rain conditions. Preliminary results exposed a major flaw of current state-of-the-art shadowing detection methods while operating during rain, presenting very poor performance in terms of false alarm for shadowing detection when no shadowing event was actually present. However, these methods still have better detection performance than the proposed IMM filter when there is no slow attenuation caused by rain.

Considerable detection performance improvements could be achieved by the proposed IMM filter approach when comparing it against current state-of-the-art methods. This is the case for a mobile terminal using an LMS channel experiencing rain fading in a GEO satellite link operating at Ka-band.

Future high throughput mobile satellite communication systems using GEO satellites at Ka-band will be able to rely on better adaptive designs based on detailed and more accurate channel state information, as those provided by filter-based detectors such as the IMM method provided in this paper. These systems will be aware of the current communication channel conditions while dealing with channel uncertainties, such as precise space and atmospheric weather models. In addition to that multiple states can be configured in order to represent specific channel conditions, with the potential to improve the performance of adaptive radios and increase the overall network cooperative aspect.

Also, some insights and details on the ITU implementations for the time series generators used in this paper were discussed, which resulted in the code made publicly available through the reference mentioned above. Future analysis will consist of taking real-world signal measurements from a Ka-band GEO satellite under the mentioned scenarios and performing the experiments described in this paper so that the results presented by this paper can be confirmed. Next, the proposed filter design must be deployed in a real-world prototype and tested on similar channel conditions asas those analyzed in this paper.

REFERENCES

[1] H. Fenech, A. Tomatis, S. Amos, V. Soumpholphakdy, and J. L. S. Merino, "Eutelsat HTS systems," *Int. J. Satellite Commun. Netw.*, vol. 34, no. 4, pp. 503–521, 2016.

[2] M. Hasan and C. Bianchi, "Ka band enabling technologies for high throughput satellite (HTS) communications," *Int. J. Satellite Commun. Netw.*, vol. 34, no. 4, pp. 483–501, 2015.

[3] (Jan. 2013). *Satellitetoday.Com Via Satellite*. [Online]. Available: http://www.satellitetoday.com/telecom/2013/01/01/payloads-seeking-the-holy-grail-of-flexibility/

[4] N. Porecki, G. Thomas, A. Warburton, N. Wheatley, and N. Metzger, "Flexible payload technologies for optimizing Ka-band payloads to meet future business needs," in *Proc. 19th Ka Broadband Commun., Navigat. Earth Observat. Conf.*, Oct. 2013, pp. 1–7.

[5] K. Butchart and R. M. Braun, "An adaptive modulation scheme for low Earth orbit satellites," in *Proc. South African Symp. Commun. Signal Process. (COMSIG)*, Sep. 1998, pp. 43–46.

[6] A. J. Goldsmith and S.-G. Chua, "Adaptive coded modulation for fading channels," *IEEE Trans. Commun.*, vol. 46, no. 5, pp. 595–602, May 1998.

[7] D. Tarchi, G. E. Corazza, and A. Vanelli-Coralli, "Adaptive coding and modulation techniques for next generation hand-held mobile satellite

communications," in *Proc. IEEE Int. Conf. Commun. (ICC)*, Jun. 2013, pp. 4504–4508.
[8] M. Bousquet *et al.*, "Cost Action 255: radiowave propagation modeling for SatCom services at Ku-Band and above final report: Impairment mitigation and performance restoration," Eur. Space Agency, Paris, France, Tech. Rep. ISSN: 0379-6566, 2002.
[9] J. Zhu and S. Roy, "Improving link layer performance on satellite channels with shadowing via delayed two-copy selective repeat ARQ," *IEEE J. Sel. Areas Commun.*, vol. 22, no. 3, pp. 472–481, Apr. 2004.
[10] R. Babaee and N. C. Beaulieu, "Cross-layer design for multihop wireless relaying networks," *IEEE Trans. Wireless Commun.*, vol. 9, no. 11, pp. 3522–3531, Nov. 2010.
[11] H. Khodakarami and F. Lahouti, "Link adaptation with untrusted relay assignment: Design and performance analysis," *IEEE Trans. Commun.*, vol. 61, no. 12, pp. 4874–4883, Dec. 2013.
[12] S. Cioni, R. de Gaudenzi, and R. Rinaldo, "Channel estimation and physical layer adaptation techniques for satellite networks exploiting adaptive coding and modulation," *Int. J. Satellite Commun. Netw.*, vol. 26, no. 2, pp. 157–188, 2008.
[13] D. R. Pauluzzi and N. C. Beaulieu, "A comparison of SNR estimation techniques for the AWGN channel," *IEEE Trans. Commun.*, vol. 48, no. 10, pp. 1681–1691, Oct. 2000.
[14] J. B. Schodorf, "EHF satellite communications on the move: Baseband considerations," Lincoln Lab., Lexington, MA, USA, Tech. Rep. 1055, 2000.
[15] R. Prieto-Cerdeira, F. Perez-Fontan, P. Burzigotti, A. Bolea-Alamanac, and I. Sanchez-Lago, "Versatile two-state land mobile satellite channel model with first application to DVB-SH analysis," *Int. J. Satellite Commun. Netw.*, vol. 29, pp. 291–315, Jun. 2010.
[16] W. Li, C. L. Law, J. T. Ong, and V. Dubey, "Ka-band land mobile satellite channel model: With rain attenuation and other weather impairments in equatorial zone," in *Proc. IEEE 51st Veh. Technol. Conf.*, vol. 3. May 2000, pp. 2468–2472.
[17] A. Rico-Alvarino, J. Arnau, and C. Mosquera, "Link adaptation in mobile satellite links: Schemes for different degrees of CSI knowledge," *Int. J. Satellite Commun. Netw.*, vol. 34, no. 5, pp. 679–694, 2015.
[18] D. S. Michalopoulos, H. A. Suraweera, and R. Schober, "Relay selection for simultaneous information transmission and wireless energy transfer: A tradeoff perspective," *IEEE J. Sel. Areas Commun.*, vol. 33, no. 8, pp. 1578–1594, Aug. 2015.
[19] M. Rieche, D. Arndt, A. Ihlow, and G. D. Galdo, "Modeling of the land mobile satellite channel considering the terminal's driving direction," *Int. J. Antennas Propag.*, vol. 2015, pp. 1–21, Dec. 2015.
[20] D. Arndt, A. Ihlow, T. Heyn, A. Heuberger, and R. Prieto-Cerdeira, "State modelling of the land mobile propagation channel for dual-satellite systems," *EURASIP J. Wireless Commun. Netw.*, vol. 228, pp. 1–21, Jul. 2012.
[21] L. E. Braten and T. Tjelta, "Semi-Markov multistate modeling of the land mobile propagation channel for geostationary satellites," *IEEE Trans. Antennas Propag.*, vol. 50, no. 12, pp. 1795–1802, Dec. 2002.
[22] Y. Hase, W. J. Vogel, and J. Goldhirsh, " Fade-durations derived from land-mobile-satellite measurements in Australia," *IEEE Trans. Commun.*, vol. 39, no. 5, pp. 664–668, May 1991.
[23] D. Tarchi, G. E. Corazza, and A. Vanelli-Coralli, "A channel state-driven ACM algorithm for mobile satellite communications," *Int. J. Satellite Commun. Netw.*, vol. 34, no. 6, pp. 787–807, 2015.
[24] M. Mardani, J. Seifali, F. Lahouti, and B. Eliasi, "Link-adaptive and QoS-provisioning cooperative ARQ—Applications to relay-assisted land mobile satellite communications," *IEEE Trans. Veh. Technol.*, vol. 60, no. 7, pp. 3192–3206, Sep. 2011.
[25] K. R. Malekshan and F. Lahouti, "Distributed cross-layer dynamic route selection in wireless multiuser multihop networks," *IEEE Trans. Wireless Commun.*, to be published. [Online]. Available: https://arxiv.org/abs/1407.5718
[26] W. G. Phoel, "Concepts for reliable satellite communications over blockage channels," in *Proc. IEEE Military Commun. Conf. (MILCOM)*, Oct. 2005, pp. 472–481.
[27] J. S. Harsini and F. Lahouti, "Quality of service constrained throughput optimisation for joint adaptive transmission with automatic repeat request over block-fading channels," *IET Commun.*, vol. 3, no. 6, pp. 1030–1040, Oct. 2009.
[28] H. A. P. Blom and Y. Bar-Shalom, "The interacting multiple model algorithm for systems with Markovian switching coefficients," *IEEE Trans. Autom. Control*, vol. 33, no. 8, pp. 780–783, Aug. 1988.
[29] N. Tudoroiu and K. Khorasani, "Satellite fault diagnosis using a bank of interacting Kalman filters," *IEEE Trans. Aerosp. Electron. Syst.*, vol. 43, no. 4, pp. 1334–1350, Oct. 2007.
[30] A. H. Sayed, *Adaptive Filters*. Hoboken, NJ, USA: Wiley, 2008.
[31] R. Labbe's Jr., *Kalman and Bayesian Filters in Python*, 2nd ed., 2015. [Online]. Available: https://github.com/rlabbe/Kalman-and-Bayesian-Filters-in-Python
[32] E. Mazor, A. Averbuch, Y. Bar-Shalom, and J. Dayan, "Interacting multiple model methods in target tracking: A survey," *IEEE Trans. Aerosp. Electron. Syst.*, vol. 34, no. 1, pp. 103–123, Jan. 1998.
[33] L. A. Johnston and V. Krishnamurthy, "An improvement to the interacting multiple model (IMM) algorithm," *IEEE Trans. Signal Process.*, vol. 49, no. 12, pp. 2909–2923, Dec. 2001.
[34] T. Sathyan and T. Kirubarajan, "Markov-jump-system-based secure chaotic communication," *IEEE Trans. Circuits Syst. I, Reg. Papers*, vol. 53, no. 7, pp. 1597–1609, Jul. 2006.
[35] T. Y. Um, J. G. Lee, S.-T. Park, and C. G. Park, "Noise covariances estimation for systems with bias states," *IEEE Trans. Aerosp. Electron. Syst.*, vol. 36, no. 1, pp. 226–233, Jan. 2000.
[36] M. Enescu, M. Sirbu, and V. Koivunen, "Recursive estimation of noise statistics in Kalman filter based MIMO equalization," in *Proc. 27th General Assembly Int. Union Radio Sci.*, Aug. 2002, pp. 1–4.
[37] Y. Li and J. Li, "Robust adaptive Kalman filtering for target tracking with unknown observation noise," in *Proc. 24th Chin. Control Decision Conf.*, May 2012, pp. 2075–2080.
[38] W.-J. Qi, P. Zhang, G.-H. Nie, and Z.-L. Deng, "Robust weighted fusion Kalman predictors with uncertain noise variances," *Digit. Signal Process.*, vol. 30, pp. 37–54, Jul. 2014.
[39] A. Assa and F. Janabi-Sharifi, "A Kalman filter-based framework for enhanced sensor fusion," *IEEE Sensors J.*, vol. 15, no. 6, pp. 3281–3292, Jun. 2015.
[40] B. Feng, F. Ma, M. Fu, and C. Yang, "Real-time state estimator without noise covariance matrices knowledge—Fast minimum norm filtering algorithm," *IET Control Theory Appl.*, vol. 9, no. 9, pp. 1422–1432, Jun. 2015.
[41] T. Kirubarajan and Y. Bar-Shalom, "Kalman filter versus IMM estimator: When do we need the latter?" *IEEE Trans. Aerosp. Electron. Syst.*, vol. 39, no. 4, pp. 1452–1457, Oct. 2003.
[42] E. Lutz, D. Cygan, M. Dippold, F. Dolainsky, and W. Papke, "The land mobile satellite communication channel-recording, statistics, and channel model," *IEEE Trans. Veh. Technol.*, vol. 40, no. 2, pp. 375–386, May 1991.
[43] D. Arndt *et al.*, "Extended two-state narrowband LMS propagation model for S-Band," in *Proc. IEEE Int. Symp. Broadband Multimedia Syst. Broadcast.*, Jun. 2012, pp. 1–6.
[44] F. Lacoste, B. M. Villacieros, R. Prieto-Cerdeira, and J. Lemorton, "SISO and MIMO enhanced 2-state modeling of the land mobile satellite channel for various frequencies, environments and elevation angles," in *Proc. 8th Eur. Conf. Antennas Propag.*, 2014, pp. 2277–2281.
[45] M. Rieche, A. Ihlow, D. Arndt, F. Perez-Fontan, and G. D. Galdo, "Modeling of the land mobile satellite channel considering the terminal's driving direction," *Int. J. Antennas Propag.*, pp. 1–21, 2015.
[46] M. Ait-Ighil *et al.*, "Simplifying the propagation environment representation for LMS channel modelling," *EURASIP J. Wireless Commun. Netw.*, vol. 1, pp. 1–20, Mar. 2012.
[47] M. Ait-Ighil *et al.*, " SCHUN - A hybrid land mobile satellite channel simulator enhanced for multipath modelling applied to satellite navigation systems," in *Proc. 7th Eur. Conf. Antennas Propag.*, 2013, pp. 692–696.
[48] S. Scalise, H. Ernst, and G. Harles, "Measurement and modeling of the land mobile satellite channel at Ku-Band," *IEEE Trans. Veh. Technol.*, vol. 57, no. 2, pp. 693–703, Mar. 2008.
[49] A. M. Al-Saegh, A. Sali, J. S. Mandeep, and A. Ismail, "Tracking and scintillation aware channel model for GEO satellite to land mobile terminals at Ku-band," *Int. J. Antennas Propag.*, pp. 1–15, 2015.
[50] NASA ACTS program, *National Aeronautics and Space Administration*, accessed on Oct. 2016. [Online]. Available: http://www.nasa.gov/centers/glenn/about/fs13grc.html
[51] RF Propagation database, *National Aeronautics and Space Administration*, accessed on Oct. 2016. [Online]. Available: https://propagation.grc.nasa.gov/background/what-are-we-measuring
[52] D. Chakraborty, F. Davarian, and W. L. Stutzman, "The Ka-band propagation measurements campaign at JPL," *IEEE Antennas Propag. Mag.*, vol. 35, no. 1, pp. 7–13, Feb. 1993.
[53] S. Ventouras *et al.*, "Large scale assessment of Ka/Q band atmospheric channel across Europe with ALPHASAT TDP5: A new propagation campaign," in *Proc. 10th Eur. Conf. Antennas Propag. (EuCAP)*, Apr. 2016, pp. 1–5.

[54] T. Kostulski and S. Reisenfeld, "Spectral analysis of experimental Ka-band propagation measurements over the australian LEO microsatellite 'FedSat'," in *Personal Satellite Services*, vol. 15. Berlin Germany: Springer, 2009, pp. 41–48.
[55] H. Fukuchi, N. Abe, T. Takahashi, and T. Asai, "Ka-band satellite communication experiments and rain attenuation measurements using WINDS," in *Proc. 7th Int. Conf. Inf., Commun. Signal Process.*, Dec. 2009, pp. 1–4.
[56] X. Boulanger, B. Gabard, L. Casadebaig, and L. Castanet, "Four years of total attenuation statistics of earth-space propagation experiments at Ka-band in Toulouse," *IEEE Trans. Antennas Propag.*, vol. 63, no. 5, pp. 2203–2214, May 2015.
[57] *Propagation Data and Prediction Methods Required for the Design of Earth-Space Telecommunication Systems*, document Rec. ITU-R P.618-12, ITU-R, Geneva, Switzerland, 2015.
[58] *Propagation Data Required for the Design of Earth-Space Land Mobile Telecommunication Systems*, document Rec. ITU-R P.681-8, ITU-R, Geneva, Switzerland, 2015.
[59] P. Ferreira and A. M. Wyglinski, *Satellite-Communications: LMS Time Series Gen GEO v1.1*. GitHub, 2015, doi: 10.5281/zenodo.44695.
[60] *Characteristics of Precipitation for Propagation Modeling*, document Rec. ITU-R P.837-6, ITU-R, Geneva, Switzerland, 2012.
[61] *Specific Attenuation Model for Rain for Use in Prediction Methods*, Rec. ITU-R P.838-3, ITU-R, Geneva, Switzerland, 2005.
[62] *Tropospheric Attenuation Time Series Synthesis*, document Rec. ITU-R P.1853-1, ITU-R, Geneva, Switzerland, 2012.
[63] *Rain Height Model for Prediction Methods*, document Rec. ITU P.839-4, ITU-R, Geneva, Switzerland, 2013.
[64] G. Corazza, *Digital Satellite Communications*. New York, NY, USA: Springer, 2007.
[65] B. Krach, A. Lehner, and A. Steingass, "Technical note on the implementation of the land mobile satellite channel model—Software usage," German Aerospace Center DLR, Köln, Germany, Tech. Rep. DLR-KN-FS-01-05, 2007.
[66] R. Faragher, "Understanding the basis of the Kalman filter via a simple and intuitive derivation," *IEEE Signal Process. Mag.*, vol. 29, no. 5, pp. 128–132, Sep. 2012.
[67] B. Feng, M. Fu, H. Ma, Y. Xia, and B. Wang, "Kalman filter with recursive covariance estimation—Sequentially estimating process noise covariance," *IEEE Trans. Ind. Electron.*, vol. 61, no. 11, pp. 6253–6263, Nov. 2014.

PAULO VICTOR RODRIGUES FERREIRA received the B.Sc. and M.Sc. degrees in electrical engineering with emphasis on telecommunications and electronics from the Federal University of Uberlandia, Brazil, in 2010 and 2012, respectively. He is currently pursuing the Ph.D. degree with the Wireless Innovation Laboratory, Department of Electrical and Computer Engineering, Worcester Polytechnic Institute, Worcester, MA, USA. He is a grantee of the Brazilian Government Scholarship Program Science without Borders.

RANDY PAFFENROTH received the degree in mathematics and degree in computer science from Boston University, and the Ph.D. degree in applied mathematics from the University of Maryland in 1999. He spent seven years as a Staff Scientist of Applied and Computational Mathematics with the California Institute of Technology. In 2006, he joined Numerica Corporation, where he held the position of Computational Scientist and Program Director. He is currently an Associate Professor of Mathematical Sciences and Associate Professor of Computer Science with Worcester Polytechnic Institute with a joint appointment in the Data Science Program. His technical interests include machine learning, signal processing, large scale data analytics, compressed sensing, and the interaction between mathematics, computer science, and software engineering, with a focus on applications in cyber-defense.

ALEXANDER M. WYGLINSKI (SM'11) received the B.Eng. and Ph.D. degrees from McGill University in 1999 and 2005, respectively, and the M.Sc. (Eng.) degree from Queen's University, Kingston, in 2000, all in electrical engineering. He is currently an Associate Professor of Electrical and Computer Engineering with Worcester Polytechnic Institute, Worcester, MA, USA, where he was the Director of the Wireless Innovation Laboratory. He has published over 35 journal papers, over 75 conference papers, nine book chapters, and two textbooks. His current research activities include wireless communications, cognitive radio, software-defined radio, dynamic spectrum access, spectrum measurement and characterization, electromagnetic security, wireless system optimization and adaptation, and cyber physical systems. He is currently being or has been sponsored by organizations, such as the Defense Advanced Research Projects Agency, the Naval Research Laboratory, the Office of Naval Research, the Air Force Research Laboratory - Space Vehicles Directorate, The MathWorks, Toyota InfoTechnology Center U.S.A., Rytheon, the MITRE Corporation, the National Aeronautics and Space Administration, and the National Science Foundation. He was a member of Sigma Xi, Eta Kappa Nu, and the ASEE.